

Department of Mathematics and Statistics

Preprint MPS-2013-02

28 January 2013

Hybrid numerical-asymptotic
approximation for high frequency scattering
by penetrable convex polygons

by

Samuel P. Groth, David P. Hewett and
Stephen Langdon



**Hybrid numerical-asymptotic approximation for high frequency
scattering by penetrable convex polygons**

SAMUEL P. GROTH, DAVID P. HEWETT AND STEPHEN LANGDON

Department of Mathematics and Statistics, University of Reading,

Whiteknights PO Box 220, Reading, RG6 6AX, UK.

strate, by comparison with an “exact” reference solution (computed using a conventional BEM with a large number of degrees of freedom), that these HNA approximation spaces can approximate the highly oscillatory solution of the transmission problem accurately and efficiently, even at high frequencies. The development of an HNA BEM based on these approximation spaces will be reported separately (Groth et al., 2013).

The main difficulty in the generalisation of the HNA methodology to the penetrable case is that the high frequency asymptotic behaviour is significantly more complicated than in the impenetrable case. In particular, the boundary of the scatterer represents the interface between two media with different wave speeds, and hence two different wavenumbers, and we expect to need to modify the ansatz (1.1) to include terms oscillating at both wavenumbers. In addition to the phenomena of reflection and diffraction that occur in the impenetrable case, in the penetrable case we observe a new phenomenon, *refraction*, which occurs when a wave propagating in the exterior medium is transmitted into the scatterer and vice versa. One key difficulty this presents is that a wave propagating inside the scatterer can undergo multiple (in fact, infinitely many) internal reflections/diffractions (this is described in more detail in §3). We therefore expect that, in order for v_m , $m = 1, 2, \dots$, to be non-

We shall assume throughout that $k_1 > 0$ and that $k_2 \in \mathbb{C}$, with $\operatorname{Re}[k_2] > 0$ and $\operatorname{Im}[k_2] \geq 0$; when $\operatorname{Im}[k_2] > 0$ the scatterer is partially absorbing. The unique solvability of this BVP is well known (see, e.g., Laliena et al. (2009, Proposition 2.1 and Corollary 3.4), which follows from results in Costabel & Stephan (1985) and Torres & Welland (1993), and also the related result Marmolejo-Olea et al. (2012, Corollary 8.5)).

Now we state a BIE formulation for (2.2)–(2.5). Note that, in this paper, we only actually solve this BIE (using a standard hp -BEM) in order to compute reference solutions for our examples in §4. The main reason for including this here is as a motivation for why we want to understand the approximation properties of the boundary solution (as mentioned in §1, we will describe a BEM based on the HNA approximation space proposed in this paper in Groth et al. (2013)). If u_1 and u_2 satisfy the BVP, then a form of Green's representation theorem holds, namely (cf., e.g., Chandler-Wilde et al. (2012a, Theorems 2.20 and 2.21))

$$u_1(\mathbf{x}) = u^i(\mathbf{x}) + \int_{\Gamma} \left(u_1(\mathbf{y}) \frac{\partial \Phi_1(\mathbf{x}, \mathbf{y})}{\partial \mathbf{n}(\mathbf{y})} \right) d\mathbf{y}$$

We remark that other BIE formulations of the transmission problem are also possible - see, e.g., Costabel & Stephan (1985), Rapún & Sayas (2008), Laliena et al. (2009), Hsiao & Xu (2011). Moreover, the approximation results we derive in the following sections are equally relevant for any direct BIE formulation, not just the particular one (2.8) described above.

3 Hybrid numerical-asymptotic approximation space

Our proposed high frequency HNA approximation space for the unknown $v = (u, \partial u / \partial \mathbf{n})$ in the BIE (2.8) is constructed in two stages. First we decompose

$$v(\mathbf{x}) = v_{go}(\mathbf{x}) + v_d(\mathbf{x})$$

to polygons/polyhedra. For polygons/polyhedra, however, the fact that the boundary Γ is composed of straight sides/faces means that the GO approximation consists of a collection of *beams* of rays propagating in the same direction and with the same amplitude. Each beam can be thought of as a plane wave with an associated propagation direction and amplitude, restricted to a certain subset of \mathbb{R}^2 . As a result, one does not need to discretise

see the discussion in Remark 3.1 below). The algorithm then tracks these limiting rays as they propagate across the interior of the scatterer, determines the points at which they re-intersect the boundary, and generates new

most important phases. For a detailed exposition of the GTD f

wedge at speed c_1 , which shed new rays propagating into the interior medium. A typical ray path is shown as a

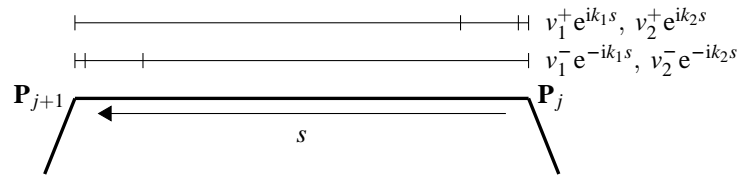


FIG. 4: Illustration of overlapping geometrically graded meshes used to approximate the amplitudes v_1^+ , v_2^+ , v_1^- , v_2^- associated with the phase functions (3.3) on a typical side Γ_j .

where $0 < \sigma < 1$ is a grading parameter. A smaller grading parameter represents a more severe grading - in all of our experiments we take $\sigma = 0.15$, as in Hewett et al. (2012). Given a vector $\mathbf{p} \in (\mathbb{N}_0)^n$, we let $P_{\mathbf{p},n}(0,L) \in \mathbb{C}^n$

with the radial distance r_i produced any beam boundaries associated with primary transmitted beams, we check whether these beam boundaries intersect the side Γ_j . If they do, we put new mesh points at the intersection points; see Figure 5 for an illustration of this procedure. Since there are at most two such beam boundaries, the side Γ_j gets subdivided into at most three elements. On each of these resulting elements we approximate w_i by a single polynomial of degree p , where p is the same as for the Approximation Space 1 amplitudes. Carrying

Space 2 to both u and $\partial u/\partial \mathbf{n}$ on Γ

accurate for each approximation space. However, on I_3 , the side in shadow, Approximation Space 2 provides a much better fit. This is not surprising, since this space also includes the effect on I_3 of the diffracted wave from P_2 , which, for this incident direction, is relatively stronger than the effects on I_1 and I_2 of the diffracted waves from P_3 and P_1

a range of values of k_1 , for $\xi = 0.05$, and for angles 1, 2, 3 and 4. Here and throughout this section we take $p = 4$ for both Approximation Spaces 1 and 2, as detailed in §3.2.2 and 05086264 Tf 223.344 0 Td [(x)-0.460706]TJ /R9 9.962

k_1	ξ	$\frac{\ u-u_{go}\ }{\ u\ }$	$\frac{\ u-U_1\ }{\ u\ }$	$\frac{\ u-U_2\ }{\ u\ }$	$\frac{\ \frac{\partial u}{\partial \mathbf{n}} - (\frac{\partial u}{\partial \mathbf{n}})_{go}\ }{\ \frac{\partial u}{\partial \mathbf{n}}\ }$	$\frac{\ \frac{\partial u}{\partial \mathbf{n}} - W_1\ }{\ \frac{\partial u}{\partial \mathbf{n}}\ }$	$\frac{\ \frac{\partial u}{\partial \mathbf{n}} - W_2\ }{\ \frac{\partial u}{\partial \mathbf{n}}\ }$
5	0.05	1.88×10^{-1}	1.66×10^{-2}	2.57×10^{-3}	1.56×10^{-1}	1.62×10^{-2}	1.97×10^{-3}
10	0.05	1.37×10^{-1}	1.03×10^{-2}	1.35×10^{-3}	7.76×10^{-2}	1.03×10^{-2}	1.26×10^{-3}
20	0.05	1.00×10^{-1}	8.41×10^{-4}	3.72×10^{-4}	5.60×10^{-2}	1.53×10^{-3}	1.35×10^{-3}
40	0.05	7.25×10^{-2}	2.23×10^{-4}	2.20×10^{-4}	4.04×10^{-2}	1.04×10^{-3}	1.04×10^{-3}
80	0.05	5.19×10^{-2}	2.58×10^{-4}	2.58×10^{-4}	2.88×10^{-2}	7.69×10^{-4}	7.69×10^{-4}
160	0.05	3.69×10^{-2}	2.31×10^{-4}	2.31×10^{-4}	2.05×10^{-2}	6.49×10^{-4}	6.49×10^{-4}
5	0.025	2.19×10^{-1}	3.03×10^{-2}	5.53×10^{-3}	1.55×10^{-1}	2.94×10^{-2}	4.14×10^{-3}
10	0.025	1.54×10^{-1}	4.09×10^{-2}	4.49×10^{-3}	9.87×10^{-2}	4.41×10^{-2}	3.73×10^{-3}
20	0.025	1.10×10^{-1}	1.15×10^{-2}	2.00×10^{-3}	6.35×10^{-2}	1.12×10^{-2}	2.22×10^{-3}
40	0.025	8.09×10^{-2}	7.01×10^{-4}	3.37×10^{-4}	4.58×10^{-2}	1.19×10^{-3}	1.04×10^{-3}
80	0.025	5.85×10^{-2}	3.42×10^{-4}	3.41×10^{-4}	3.30×10^{-2}	7.69×10^{-4}	7.69×10^{-4}
160	0.025	4.19×10^{-2}	2.80×10^{-4}	2.80×10^{-4}	2.35×10^{-2}	6.44×10^{-4}	6.44×10^{-4}
5	0.0125	2.48×10^{-1}	4.05×10^{-2}	8.02×10^{-3}	1.90×10^{-1}	3.94×10^{-2}	5.96×10^{-3}
10	0.0125	1.84×10^{-1}	7.88×10^{-2}	9.46×10^{-3}	1.35×10^{-1}	8.07×10^{-2}	7.69×10^{-3}
20	0.0125	1.28×10^{-1}	4.53×10^{-2}	9.42×10^{-3}	8.05×10^{-2}	4.41×10^{-2}	8.49×10^{-3}
40	0.0125	9.13×10^{-2}	1.05×10^{-2}	2.66×10^{-3}	5.03×10^{-2}	1.01×10^{-2}	2.56×10^{-3}
80	0.0125	6.69×10^{-2}	1.87×10^{-3}	1.79×10^{-3}	3.61×10^{-2}	1.04×10^{-3}	9.07×10^{-4}
160	0.0125	4.84×10^{-2}	7.52×10^{-4}	7.52×10^{-4}	2.60×10^{-2}	6.68×10^{-4}	6.68×10^{-4}
5	0	2.57×10^{-1}	5.30×10^{-2}	1.16×10^{-2}	2.30×10^{-1}	5.17×10^{-2}	8.57×10^{-3}
10	0	2.15×10^{-1}	1.43×10^{-1}	1.95×10^{-2}	1.99×10^{-1}	1.49×10^{-1}	1.60×10^{-2}
20	0	1.79×10^{-1}	1.48×10^{-1}	2.82×10^{-2}	1.65×10^{-1}	1.47×10^{-1}	2.25×10^{-2}
40	0	1.50×10^{-1}	1.34×10^{-1}	3.07×10^{-2}	1.39×10^{-1}	1.31×10^{-1}	2.37×10^{-2}
80	0	1.25×10^{-1}	1.17×10^{-1}	3.17×10^{-2}	1.17×10^{-1}	1.13×10^{-1}	2.30×10^{-2}
160	0	1.04×10^{-1}	1.00×10^{-1}	2.81×10^{-2}	9.80×10^{-2}	9.58×10^{-2}	2.07×10^{-2}

Table 1: Relative errors in approximation of u and $\partial u/\partial \mathbf{n}$, using GO and each approximation space, for a range of values of

k_1	ξ	$\frac{\ u-U_1\ }{\ u\ }$
-------	-------	---------------------------

+

+

+

+

A.2 An interface between two media with arbitrary absorption

We now consider the canonical problem of the reflection/refraction of an incident plane wave of the general form (A.3) propagating in a medium with refractive index $\mu_1 + i\xi_1$ at a planar interface with a second medium with refractive index $\mu_2 + i\xi_2$. We assume that in the first medium the field takes the form $u = u^i + u^r$, where u^i is the incident plane wave and u^r is a reflected plane wave, and that in the second medium the field takes the form $u = u^t$, where u^t is a transmitted plane wave. We also assume that both the total field u and its normal derivative are continuous across the interface, which implies that, on the interface,

$$u^i + u^r = u^t \quad \text{and} \quad \frac{\partial u^i}{\partial \mathbf{n}} + \frac{\partial u^r}{\partial \mathbf{n}} = \frac{\partial u^t}{\partial \mathbf{n}}, \quad (\text{A.6})$$

where \mathbf{n} is a vector normal to the interface. We write the waves u^i , u^r and u^t in the general form (A.3) as:

$$\begin{aligned} u^i &= A^i \exp\{ik_0(D_i \mathbf{d}^i + iE_i \mathbf{e}^i) \cdot \mathbf{x}\}, \\ u^r &= A^r \exp\{ik_0(D_r \mathbf{d}^r + iE_r \mathbf{e}^r) \cdot \mathbf{x}\}, \\ u^t &= A^t \exp\{ik_0(D_t \mathbf{d}^t + iE_t \mathbf{e}^t) \cdot \mathbf{x}\}, \end{aligned} \quad (\text{A.7})$$

where we have assumed a priori the same ‘‘apparent refractive index’’ for the reflected wave as for the incident wave. Given the parameters A^i , \mathbf{d}^i , \mathbf{e}^i , D_i and E_i describing the incident wave, we wish to determine the parameters A^r , A^t , \mathbf{d}^r , \mathbf{e}^r , \mathbf{d}^t , \mathbf{e}^t , D_t and E_t

or, in the notation of Figure 10, simply as



Having justified the choice of the positive square root in (A.21), we can state the formulae for D_t and E_t :

$$\begin{aligned} D_t &= \sqrt{\frac{1}{2} \left(\mu_2^2 - \xi_2^2 + \tilde{D}_i^2 + \tilde{E}_i^2 + \sqrt{(\mu_2^2 - \xi_2^2 - \tilde{D}_i^2 + \tilde{E}_i^2)^2 + 4(\tilde{D}_i \tilde{E}_i - \mu_2 \xi_2)^2} \right)}, \\ E_t &= \sqrt{D_t^2 + \xi_2^2 - \mu_2^2}, \end{aligned} \tag{A.26}$$

where the non-negative square root is taken in both equations.

A.2.4 Normal components of transmitted direction vectors

- When $|\mathbf{d}^i \cdot \mathbf{t}| = 1$ (i.e. $\mathbf{d}^i \cdot \mathbf{n} = 0$), we take \mathbf{d}^i to point into the second medium. We note that if $E_i = 0$ then $v_i = 0$, and so $R = -1$ and $T = 0$ (i.e. the solution is identically zero).

We now turn to \mathbf{e}^i

- L. Bi, et al. (2011). ‘Scattering and absorption of light by ice particles: Solution by a new physical-geometric optics hybrid method’. *J. Quant. Spectrosc. Ra.* **112**:1492–1508.
- M. Born & E. Wolf (1997). *Principles of Optics*. Cambridge University Press.
- V. A. Borovikov & B. Y. Kinber (1994). *Geometrical Theory of Diffraction*. IEE.
- J. J. Bowman, et al. (1969). *Electromagnetic and Acoustic Scattering by Simple Shapes*. North-Holland, Amsterdam.
- L. M. Brekhovskikh (1960). *Waves in Layered Media*. Academic Press.
- B. Budaev & D. Bogy (1999). ‘Rigorous solutions of acoustic wave diffraction by penetrable wedges’. *J. Acoust. Soc. Am.* **105**:74.
- S. N. Chandler-Wilde, et al. (2012a). ‘Numerical-asymptotics boundary integral methods in high-frequency acoustic scattering’. *Acta Numer.* pp. 89–305.
- S. N. Chandler-Wilde, et al. (2012b). ‘A high frequency boundary element method for scattering by a class of nonconvex obstacles’. *Submitted for publication - University of Reading preprint MPS-2012-04* .
- S. N. Chandler-Wilde & S. Langdon (2007). ‘A Galerkin boundary element method for high frequency scattering by convex polygons’. *SIAM J. Numer. Anal.* **45**(2):610–640.
- S. N. Chandler-Wilde, et al. (2012c). ‘A high frequency boundary element method for scattering by convex polygons with impedance boundary conditions’. *Commun. Comput. Phys.* **11**(2):575–593.
- P. C. Y. Chang, et al. (2005). ‘Ray tracing in absorbing media’. *J. Quant. Spectrosc. Ra.* **96**:327–341.
- D. Colton & R. Kress (1983). *Integral Equation Methods in 1299(3)0.439sial. tbsP96*

